Sains Malaysiana 55(6)(2026): 986-997
http://doi.org/10.17576/jsm-2026-5506-04

Graphene Oxide Derivatives as Advanced Nanocarriers against Breast Cancer Cells

(Terbitan Grafena Oksida sebagai Pembawa Nano Termaju terhadap Sel Kanser Payudara)

UNG YEE TZE[1], NOR AMIN HASSAN[1], KHOR BOON KEAT[2,3], VIKNESWARAN MURUGAIYAH[2,3], BEH KHI POAY[4], BATOUL DHAINI[5], SAMIR ACHERAR[5], CÉLINE FROCHOT[5] & AMIRAH MOHD GAZZALI[1,*]

[1]*School of Pharmaceutical Sciences, Universiti Sains Malaysia, Penang 11800, Malaysia*
[2]*Department of Pharmacology, School of Pharmaceutical Sciences, Universiti Sains Malaysia, Penang, Malaysia*
[3]*Centre for Drug Research, Universiti Sains Malaysia, Penang, Malaysia*
[4]*School of Physics, Universiti Sains Malaysia (USM), 11800, Penang, Malaysia*
[5]*Université de Lorraine, CNRS, LRGP, F-54000 Nancy, France*

Received: 1 November 2025/Accepted: 20 May 2026

ABSTRACT

Graphene-based nanomaterials have attracted significant attention as drug delivery platforms due to their high surface area, ease of functionalization and biocompatibility. This study investigates and compares graphene oxide (GO) and reduced graphene oxide (rGO) for their efficiency in loading methylene blue (MB) and their *in vitro* cytotoxic effects on MCF-7 breast cancer cells. GO and rGO were synthesized via improved Hummers' method and chemical reduction with ascorbic acid, respectively. The resulting nanomaterials were characterized for functional groups and drug release behavior at physiological (pH 7.4) and acidic (pH 4.5) conditions. Successful formation of GO-MB and rGO-MB complexes was confirmed by spectral shifts in FTIR. *In vitro* drug release studies demonstrated a pH-responsive profile, with complete release from GO-MB and rGO-MB occurring within 24 h and 20 min, respectively, at pH 4.5. *In vitro* cytotoxicity evaluation against MCF-7 breast cancer cells showed enhanced cytotoxic effect of GO-MB on MCF-7, while maintaining lower toxicity towards normal human fibroblast (Hs27) cells. These findings exhibit the superior performance of GO as a drug carrier over rGO, showing its potential for safe and effective anti-breast cancer therapy.

Keywords: Breast cancer; graphene oxide; methylene blue; reduced graphene oxide

ABSTRAK

Bahan nano berasaskan grafena telah menarik perhatian yang meluas sebagai platform penghantaran ubat disebabkan oleh luas permukaan yang tinggi, kemudahan kefungsian serta biokeserasian yang baik. Kajian ini meneliti dan membandingkan grafena oksida (GO) dan grafena oksida terkurang (rGO) dari segi kecekapan pemuatan metilena biru (MB) serta kesan sitotoksik *in vitro* terhadap sel kanser payudara MCF-7. GO dan rGO masing-masing telah disintesis melalui kaedah Hummers yang dipertingkatkan dan penurunan kimia menggunakan asid askorbik. Bahan nano yang dihasilkan telah dicirikan bagi menentukan kumpulan berfungsi serta tingkah laku pelepasan ubat pada keadaan fisiologi (pH 7.4) dan berasid (pH 4.5). Pembentukan kompleks GO-MB dan rGO-MB telah disahkan melalui anjakan spektrum dalam analisis FTIR. Kajian pelepasan ubat *in vitro* menunjukkan profil pelepasan yang peka terhadap perubahan pH dengan pelepasan lengkap daripada GO-MB dan rGO-MB masing-masing dicapai dalam tempoh 24 jam dan 20 minit pada pH 4.5. Penilaian sitotoksisiti secara *in vitro* terhadap sel MCF-7 menunjukkan GO-MB menghasilkan kesan sitotoksik yang lebih tinggi terhadap sel kanser tersebut, sambil mengekalkan ketoksikan yang lebih rendah terhadap sel fibroblas manusia normal (Hs27). Keputusan ini membuktikan bahawa GO mempunyai keupayaan yang lebih unggul sebagai pembawa ubat berbanding rGO, sekali gus menyerlahkan potensi GO sebagai agen penghantaran ubat yang selamat dan berkesan untuk terapi anti-kanser payudara.

Kata kunci: Kanser payudara; metilena biru; oksida grafena; oksida grafena terturun

INTRODUCTION

Breast cancer is a chronic, non-communicable disease that predominantly affects women. According to the World Health Organization (WHO), as of 2022, breast cancer was the most common cancer in women in 157 countries out of 185, with 99% of cases occurring in women and approximately 0.5-1% occurring in men (WHO 2024). Standard therapeutic approaches for breast cancer include chemotherapy, radiation therapy, surgical intervention, as well as targeted and hormonal drug therapies. Despite their

efficacy, these treatments often result in adverse effects. Chemotherapy can lead to side effects such as nausea and cellular toxicity, while radiation may cause post-operative complications, including fatigue, pain, and localized swelling (National Cancer Institute 2020). Moreover, the low specificity of conventional chemotherapeutic agents remains a significant challenge in the development of effective anticancer treatments (Joyce Nirmala et al. 2023).

Graphene-based nanomaterials have gained considerable attention in drug delivery research due to their excellent biocompatibility and exceptionally large surface area, which enables more efficient drug loading and transport (Asif et al. 2022; Liu 2021). Graphene oxide (GO) is an oxygenated form of graphene, which contains various functional groups such as carboxylic acids, epoxides and hydroxyls. The functionalization of GO with oxygenated groups improves its biocompatibility, solubility, and hydrophilicity, making it potentially useful for drug delivery applications (Yaghoubi et al. 2022; Yanikoglu et al. 2024). Reduced graphene oxide (rGO) on the other hand has fewer oxygen-containing functional groups, rendering it more hydrophobic than GO.

Previous studies have demonstrated that the incorporation of anticancer agents onto GO and rGO can enhance the elimination of cancer cells (Kasturi et al. 2016). However, despite the growing interest in graphene-based drug delivery systems, direct comparative evaluation of GO and rGO in terms of drug loading efficiency, release kinetics and cytotoxic selectivity remains limited. This study reports the synthesis and characterization of methylene blue (MB)-loaded GO and rGO and their potential as drug delivery carrier. The physicochemical properties of the resulting nanomaterials were characterized, and drug release studies were conducted under physiological (pH 7.4) and acidic (pH 4.5) conditions to assess pH-responsive behavior. Additionally, *in vitro* cytotoxicity was evaluated using normal human fibroblasts (Hs27) and breast cancer cells (MCF-7) to determine the biocompatibility and therapeutic potential of both unloaded and MB-loaded systems.

MATERIALS AND METHODS

MATERIALS

Synthetic graphite powder (< 20 μm), potassium permanganate ($KMnO_4$) and sodium acetate were purchased from Sigma-Aldrich, Co., St. Louis, MO, USA; hydrogen peroxide (H_2O_2) 30%, sulfuric acid (H_2SO_4) 95-98%, ortho-phosphoric acid (H_3PO_4) 85%, hydrochloric acid (HCl) 37%, sodium chloride (NaCl) were purchased from R&M Chemicals, Bhopal, Madhya Pradesh, India; ascorbic acid was purchased from HmbG Chemicals, Hamburg, Germany; sodium hydroxide (NaOH) was purchased from BDH, Merck, UK; acetic acid (CH_3COOH) and dimethyl sulfoxide (DMSO) were purchased from Systerm, Selangor, Malaysia; potassium bromide (KBr) was purchased from Uvasol, Merck, Darmstadt, Germany; potassium chloride (KCl) and monopotassium phosphate (KH_2PO_4) were purchased from Bendosen, Selangor, Malaysia; disodium phosphate (Na_2HPO_4) was purchased from Chemiz, Selangor, Malaysia; methylene blue (Systemic name: 3,7-bis(Dimethylamino)-phenothiazine-5-ium chloride) was purchased from AJAX Finechem chemicals (UNILAB), Sydney, Australia. Dulbecco's Modified Eagle Medium (DMEM) high glucose, penicillin-streptomycin solution, 10,000 units/mL, 2.5 g/L-trypsin/1 mmol/L-EDTA solution were purchased from Nacalai Tesque, Nakagyo-ku, Kyoto, Japan, thiazolyl blue tetrazolium bromide, MTT (3-(4,5-Dimethylthiazol-2-yl)-2,5-diphenyltetrazolium bromide) was purchased from Alfa Aesar, Lancashire, UK. Fetal bovine serum (FBS) was purchased from TICO Europe, DJ, Amstelveen, the Netherlands.

GRAPHENE OXIDE (GO) SYNTHESIS

GO was synthesized via the improved Hummers method (Marcano et al. 2010). Briefly, a mixture of concentrated H_2SO_4 and H_3PO_4 was premixed in a ratio of 9:1 (90 mL: 10 mL) and was added gradually into 1 g graphite powder prepared in a 1000 mL beaker, followed by the slow addition of 6 g $KMnO_4$ into the solution under stirring conditions. The overall temperature of the mixture was maintained below 50 °C. The mixture was continuously stirred for 48 h to allow the oxidation process to occur. Then, the mixture was added to 100 mL of ice prepared in a beaker, followed by the addition of 30% H_2O_2 solution to cease the reaction by reducing the residual $KMnO_4$ into soluble manganese sulfate ($MnSO_4$) (Habte & Ayele 2019). The mixture was then centrifuged at 4000 rpm for 20 min, and the supernatant was discarded. The remaining solid was washed with 30% HCl and centrifuged at 4000 rpm for 20 min. This step was repeated a few times to remove excess sulfate ions, and the supernatant was decanted away after each wash. In the next step, distilled water was added to the residuals and continuously washed until the pH reached 6-7. For each wash, the solution was centrifuged for 30 min at 4000 rpm, and the supernatant was discarded. The washed GO solution was then freeze-dried, and the yield percentage was calculated. The steps were repeated three times to obtain the average final yield for GO. Reaction yield: 94.5%. Physical character: Dark solid powder. FTIR (KBr, 400-4000 cm^{-1}): 3404, 1716, 1622, 1225, 1043. EDX (%): C (53.75 ± 6.01), O (46.25 ± 6.01).

REDUCED GRAPHENE OXIDE (RGO) SYNTHESIS

The rGO was prepared from GO through the chemical reduction method using ascorbic acid (AA) (Andrijanto et al. 2016). Firstly, 0.25 mg/mL of GO was dispersed in distilled water and sonicated for 10 min using a water bath sonicator until a homogenous suspension was obtained. Then, the solution was stirred at 600 rpm and heated up to 100 °C, followed by the slow addition of 20 mg/mL of

AA. Subsequently, 3 M of NaOH was added to the solution until the pH reached 10-11. The solution was allowed to continuously stir for 2 h, centrifuged, and freeze-dried to obtain the rGO powder. The steps were repeated three times to obtain the average final yield for rGO (Equation 1). Reaction yield: 56.1%. Physical character: Dark brown solid powders. FTIR (KBr, 400-4000 cm^{-1}): 3383, 1648, 1208. EDX (%): C (55.34 ± 4.22), O (35.42 ± 4.88), Na (9.23 ± 0.65).

DRUG LOADING OF GO-MB AND rGO-MB

GO-MB and rGO-MB were prepared according to the self-assembly method (Ma et al. 2020). First, 20 mg of the carrier was dispersed in 50 mL of distilled water, followed by bath sonication for 2 h. Then, the MB solution at different concentrations (0.04, 0.08, 0.12, 0.16, and 0.83 mg/mL) was slowly added into the dispersion solution and magnetically stirred for 2 h in the dark at room temperature. The mixture was then centrifuged for 30 min at 4000 rpm three times to eliminate the unloaded drug, and the supernatant was discarded. The pellet was then freeze-dried. The steps were done in triplicate to obtain the average drug loading percentage and encapsulation efficiency (Farmoudeh et al. 2020). Reaction yield: [DL %] GO-MB 18.6% ± 0.20, rGO-MB 14.3% ± 0.24. [EE% %] GO-MB 93.4% ± 0.06, rGO-MB 72.1% ± 0.09. Physical character: Dark solid powder. FTIR (KBr, 400-4000 cm^{-1}) (GO-MB): 3355, 1731, 1598, 1487, 1387, 1241, 1069. FTIR (KBr, 400-4000 cm^{-1}) (rGO-MB): 3420, 1640, 1588, 1381, 1199.

FOURIER TRANSFORM INFRARED SPECTROSCOPY (FT-IR)

FT-IR analysis was conducted by Thermo Scientific Nicolet Nexus 470 FT-IR spectrophotometer (Thermo Scientific, Waltham, MA, USA) and was set to take sixteen scans of each sample in the 400 to 4000 cm^{-1} regions with a resolution of 2 cm^{-1} using the KBr Pellet technique to investigate the chemical composition for GO, GO-MB, rGO, rGO-MB, MB, and graphite (Kim et al. 2020; Sakin Omer et al. 2018). Briefly, 1 mg of the sample was mixed with 100 mg of KBr. The mixture was mixed well via a grinding process using a set of mortar and pestle, followed by the compression of the sample under pressure to form a pellet. The results were analyzed via Omnic™ Spectra Software (Thermo Nicolet, USA). All the samples were done in duplicate.

SCANNING ELECTRON MICROSCOPE (SEM) AND ENERGY DISPERSIVE X-RAY (EDX)

SEM and EDX results were recorded by FEI Quanta 650 FEG SEM (FEI, USA) to determine the morphology of GO, rGO and graphite (Zhao et al. 2019). Each of the samples was coated with platinum and analyzed in both secondary electron and backscattered modes. The samples were analyzed under the magnification of 500X and 10,000X for GO and rGO, while for graphite it was 10,000X.

In vitro DRUG RELEASE STUDY

The release study of MB from GO-MB and rGO -MB were determined using the dialysis membrane method by dispersing GO-MB (equivalent MB: 0.93 mg) and rGO-MB (equivalent MB: 0.73 mg) in 4 mL of buffer at two different pH values- PBS buffer (pH 7.4) and acetate buffer (pH 4.5). The solution was transferred into a dialysis bag with a 12-14 kDa molecular weight cut off (Spectrum Laboratories, Inc., Rancho Dominguez, CA) and was immersed in 300 mL of buffer in a Varian VK7000 dissolution tester (Agilent Technologies, California, USA) maintained at a temperature of 37 °C with a rotating paddle at 100 rpm. At predetermined time points, 2 mL of buffer was retrieved to determine the amount of drug release, and an equal volume of fresh buffer was replenished immediately. The solution was analyzed at 663 nm using UV-VIS spectroscopy (Thermo Scientific GENESYS 30, Thermo Scientific, Waltham, MA, USA) to calculate the cumulative percentages of released MB from GO and rGO (Ma et al. 2020).

CELL CULTURE

Human fibroblast cells (Hs27) and human breast cancer cells (MCF-7) were obtained from ATCC, USA. The cells were cultured in DMEM high glucose medium supplemented with 10% FBS, and 1% penicillin-streptomycin and were incubated in a humidified incubator at 37 °C under 5% CO_2 and 90% humidified atmosphere. Upon 80% confluency, the cells were washed with PBS twice, followed by adding 0.5 mL of L-trypsin EDTA solution for 1-3 min to detach the cells. The trypsin activity was stopped by adding 5 mL of complete medium and centrifuging at 12,000 rpm for 2-3 min. The supernatant was removed, and 10 mL of complete medium was added. Resuspension was done, and 5 mL of the cell solution was added to a 25 cm^2 culture flask. More than 2 passages from the freezing stock were done before the cells were used in the following assay (Ramachandran et al. 2022).

In vitro CYTOTOXICITY ASSAY

MTT assay was employed to evaluate the viability of Hs27 and MCF-7 cells following treatment with MB, GO, GO-MB, rGO, and rGO-MB at different concentrations in the absence of light irradiation. Briefly, Hs27 and MCF-7 cells at a density of 5×10^4 cells/mL were seeded in 96-well plates and incubated overnight. Upon confirmation of the cell confluency, the cells were then treated with DMEM cell culture medium containing 1% FBS and different concentrations of MB, GO, GO-MB, rGO, and rGO -MB (0, 3.125, 6.25, 12.5, 25, and 50 µg/mL) which represented the final concentrations of the reaction mixture for 48 h at 37 °C in CO_2 incubator under dark condition. Upon completing the incubation, 10 µL of MTT solution (5 mg/mL) was added, and the cells were further incubated for 4 h at 37 °C. Then, 100 µL of DMSO was added into each well after the removal of media and agitated for

15 min to dissolve the purple formazan crystals. The absorbance of each well at 570 nm and 630 nm as the reference wavelength was analyzed using a Multiskan Go UV microplate reader (ThermoFisher Scientific, Waltham, MA, USA) (Ramachandran et al. 2022). The cells incubated with the cell culture medium without treatment were referred to as the control group. Positive control was also included with 5-fluorouracil (5-FU) to compare the effectiveness between the chemo-drug and the samples. The cell viability and selectivity index (SI) were calculated according to Equations (1) and (2).

$$\text{viable cells (\%)} = \frac{Absorbance\ (treated) - Absorbance\ (Blank)}{Absorbance\ (Untreated) - Absorbance\ (Blank)} x\ 100\% \quad (1)$$

$$\text{Selectivity Index, SI (\%)} = \frac{Mean\ IC50\ against\ normal\ cells}{Mean\ IC50\ against\ tumour\ cells} \quad (2)$$

STATISTICAL ANALYSIS

Drug encapsulation efficiency was analyzed via Student's *t*-test to determine the significant differences between group means (GO-MB and rGO-MB). A normality test was performed, and there was no significant difference that could be observed. The results for the cytotoxic study are presented as mean ± SD of two independent experiments, each performed in triplicate. A normality test was performed for the data obtained, and no significant difference could be observed and thus, the data were considered normally distributed, and a parametric test was used to analyze the results. The statistically significant differences between group means (control cells, Hs27 and MCF-7 cells) were analyzed through Student's *t*-test and two-way analysis of variance (ANOVA), followed by Bonferroni post hoc test via GraphPad Prism 8.0 (GraphPad, San Diego, CA) software. A p-value of < 0.05 was considered statistically significant.

RESULTS AND DISCUSSION

FT-IR SPECTROSCOPY ANALYSIS

FT-IR spectroscopy was conducted to determine the structural features, and functional groups present in graphite, GO, rGO, GO-MB, rGO-MB, and MB. The results are summarized in Table 1. The FT-IR spectrum of GO showed characteristic peaks at 3404 cm^{-1} (O-H stretching), 1716 cm^{-1} (C=O stretching), 1622 cm^{-1} (C=C stretching), 1225 cm^{-1} (C-O-C epoxy), and 1043 cm^{-1} (C-O stretching), confirming the successful oxidation of graphite and the introduction of oxygen-containing functional groups. In contrast, graphite exhibited minimal oxygen-related peaks, indicating its largely non-oxidized structure.

A notable shift in the O-H stretching vibration band was observed upon loading of MB onto GO, whereby the peak at 3404 cm^{-1} in GO shifted to 3355 cm^{-1} in GO-MB. This shift suggests hydrogen bonding or electrostatic interactions between the hydroxyl groups of GO and MB. Additionally, the C=C stretching vibration peak of GO (1622 cm^{-1}) was shifted to 1598 cm^{-1} in GO-MB, which is very close to MB's intrinsic C=C peak at 1597 cm^{-1}. This could be attributed to the π-π stacking interactions between the aromatic domains of GO and MB, which may cause delocalization of π electrons in GO, weakening the C=C bonds in GO and shifting the stretching frequency towards MB (Zhang et al. 2010). This finding strongly supports the successful loading of MB onto GO via non-covalent interactions, which is a commonly reported mechanism for adsorption onto graphene-based materials.

SCANNING ELECTRON MICROSCOPE (SEM) AND ENERGY DISPERSIVE X-RAY (EDX)

SEM analysis was done to observe the morphology of the samples. The morphological characteristics of graphite, GO, and rGO are shown in Figure 1. The surface of graphite in Figure 1(A) showed stacked layers, while the surface of GO in Figure 1(B) showed random aggregates with multi-layer sheets. The stacking nature of GO appeared after drying, which was also reported in a previous study (De Silva, Huang & Yoshimura 2018). The wrinkled and

TABLE 1. Summary of the peak intensity shown in FT-IR spectra

Sample	Functional groups (cm^{-1})					
	Hydroxyl stretching (O-H)	Carbonyl stretching (C=O)	Epoxy group (C-O-C)	C-N	Alkoxy stretching (C-O)	C=C
Graphite	3394	-	-	-	1030	-
GO	3404	1716	1225	-	1043	1622
GO-MB	3355	1731	1241	1487, 1387	1069	1598
rGO	3383	-	1208	-	-	1648
rGO-MB	3420	-	1199	1588, 1381	-	1640
MB	3416	-	-	1489, 1394	-	1597

layered flakes indicates that the graphene layers were oxidized into GO during the oxidation process (Hidayah et al. 2017). This observation is consistent with the FT-IR results, which confirm the presence of oxygen-containing functional groups in GO.

As for rGO in Figure 1(C), the surface morphology showed the formation of a highly distorted surface after the reduction process, which was able to prevent face-to-face stacking of graphene layers in rGO (Arias et al. 2020). A comparison between rGO with GO found that the surface of rGO appeared more porous based on qualitative observation of SEM images, showing increased surface roughness and void-like structures compared to GO (Azizighannad & Mitra 2018; De Silva, Huang & Yoshimura 2018; Faniyi et al. 2019). A noticeable reduction in the intensity of oxygen-related peaks in rGO, particularly the C=O and C-O stretching bands indicates the partial removal of oxygen-containing functional groups during the reduction process. The decrease in these functional groups supports the transformation of GO into a reduced structure, consistent with the observed morphological changes in SEM.

The EDX analysis showed that graphite was mainly composed of carbon (98%) and a small amount of oxygen (1%). As for GO, it was composed of carbon (51%) and oxygen (49%). Previous study reported that the C/O ratio of GO using Hummers' method is 1.8-2.5, while for the modified or improved Hummers' method, the ratio is 0.7-1.3 (Chasanah et al. 2022). The GO synthesized throughout this study by employing the improved Hummers' method showed a ratio of within the range reported (1.3:1) and the formation of highly oxidized GO using Hummers' method is usually reported when compared to the Brodie method which may be due to the differences in the acid medium used (H_2SO_4 or HNO_3) and the type of salt used ($KMnO_4$ or $KClO_3$) (Botas et al. 2013). Other studies also reported that the amount of the $KMnO_4$ used in the improved Hummers' method was doubled as compared to the Hummers' method and the modified Hummers' method, which may give a higher oxidation degree of GO (Zaaba et al. 2017).

A comparison between GO and rGO showed a modest decrease in oxygen content from 49% to 42%, indicating partial removal of oxygen-containing functional groups during the reduction process. This suggests that ascorbic acid, as a mild reducing agent, results in incomplete reduction of GO (Tewatia et al. 2021). The relatively small difference in oxygen content may also be attributed to the limitations of EDX analysis, which provides semi-quantitative surface composition and may not fully reflect the extent of reduction (Goldstein et al. 2017). Nevertheless, the observed decrease supports the successful conversion of GO to rGO.

In vitro DRUG RELEASE STUDY

The release profile of MB from GO and rGO microparticles was investigated under physiological (pH 7.4) and acidic (pH 4.5) conditions at 37 °C (Figure 2). Under pH 7.4, MB exhibited a gradual release from GO, reaching 61% over 24 h. In contrast, at acidic pH 4.5, the release was faster and more complete, with 100% of MB released within 24 h. The initial burst release observed may be attributed to the presence of MB molecules that were adsorbed or loosely bound to the GO surface.

For rGO, a markedly faster release was observed under both pH conditions. At pH 7.4, 87% of the MB was released within just 20 min, while complete release (100%) was achieved at pH 4.5 in the same time frame. This rapid release is likely due to weaker interactions between the hydrophilic MB and the more hydrophobic surface of rGO, impacting the binding affinity and desorption of the drug from rGO surfaces.

According to van Oss (2008), hydrophilic and hydrophobic particles tend to attract each other in aqueous environments, though this interaction is weaker than that of two hydrophobic entities. Consequently, the relatively weak binding affinity between the hydrophilic drug MB and the hydrophobic rGO surface facilitates its rapid release compared to GO, which is more hydrophilic. This observation aligns with the finding from this study, whereby MB was released significantly faster from rGO than from GO.

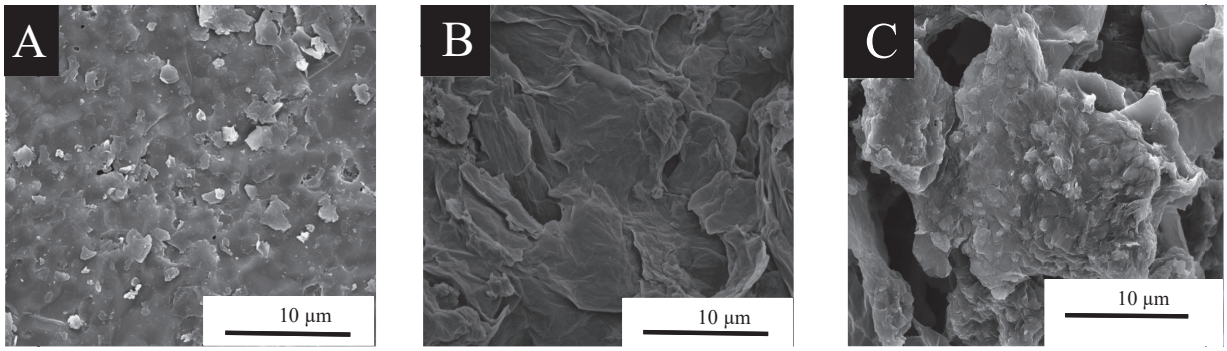

FIGURE 1. SEM results of graphite (A), GO (B) and rGO (C)

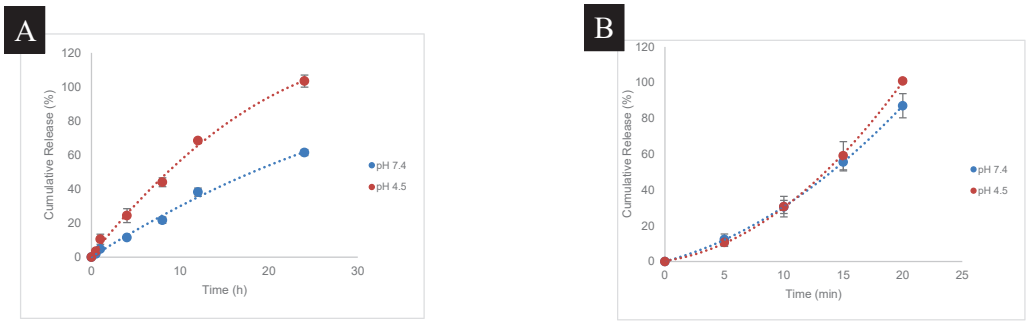

FIGURE 2. The release of MB at pH 4.5 (red line) and pH 7.4 (blue line). (A) Release curve of MB from GO-MB; total duration = 24 h and (B) Release curve of MB from rGO-MB; total duration = 20 min

The enhanced release of MB under acidic conditions for both GO and rGO may be attributed to the high concentration of H^+ ions, which promote the desorption of cationic MB. The H^+ ions can competitively displace MB from the microparticle surface (Ma et al. 2020), while simultaneously converting ionized carboxyl groups ($-COO^-$) to their protonated form (-COOH). This protonation weakens the interactions between MB and the GO/rGO surface, facilitating drug release. Previous studies also support the occurrence of proton exchange between the nanocomposite and the surrounding medium during the desorption process. Specifically, under acidic conditions, the protonation of carboxyl groups on GO and rGO disrupts the ionic bonding with positively charged MB, promoting its release (Hoseini-Ghahfarokhi et al. 2020; Wu & Jiang 2018). These findings highlight the potential of pH-responsive drug delivery at tumor sites, which are characteristically more acidic than normal physiological environments, enhancing targeted therapy and reducing systemic side effects.

In contrast, at physiological conditions (pH 7.4), carboxyl groups on GO exist predominantly in their ionized form ($-COO^-$), which favors stronger electrostatic interactions and π-π stacking with MB (Ma et al. 2020; Salahuddin et al. 2021). According to Martis, Parushuram and Sangappa (2022), higher pH levels may increase the formation of negatively charged $-COO^-$ groups due to deprotonation and enhance the adsorption of hydroxide ions on the GO surface, increasing its negative charge density. This, in turn, strengthens the interaction with MB. However, in the case of rGO, the drug release profile showed minimal difference between acidic and neutral pH conditions, likely due to the inherently weak interaction between MB and the rGO surface. As such, GO demonstrated superior performance compared to rGO, likely due to its higher density of oxygen-containing functional groups that enhanced hydrophilicity, drug loading capacity and electrostatic interaction with methylene blue, making it a more suitable candidate for pH-responsive drug delivery applications.

In vitro CYTOTOXICITY ASSAY

The cytotoxic effect and the IC_{50} values of GO, GO-MB, rGO, rGO-MB, and MB were evaluated *in vitro* on MCF-7 breast cancer cells and Hs27 human fibroblast cells for 48 h. The cytotoxicity of MB-loaded microparticles is an important evaluation to determine the *in vitro* safety of the microparticles. Theoretically, living cells would convert the MTT compound into an insoluble formazan that would be solubilized using DMSO (Ghasemi et al. 2021). Hs27 is the human fibroblast cells, which represent the non-cancerous cells, while MCF-7 represents the breast cancer cells.

In general, a concentration-dependent cytotoxicity was observed. GO showed negligible cytotoxicity towards Hs27 cells, while for MCF-7 cells, a significant reduction in cell viability was shown when tested at the highest concentration of 50 µg/mL ($p < 0.01$). This finding is in agreement with a report by Kaur et al. (2025), in which the authors observed that graphene was non-toxic to fibroblasts, but exhibited moderate cytotoxicity on cervix cancer cells (HeLa). On the other hand, rGO showed negligible cytotoxicity towards MCF-7 cells but a significant cytotoxic effect on Hs27 cells (25 and 50 µg/mL, $p < 0.001$) (Figure 3). This finding highlights the biocompatibility of GO towards normal cells and its cytotoxicity on MCF-7 cells.

Half-maximal inhibitory concentration (IC_{50}) is defined as the concentration of a drug required to inhibit a biological process by half, and it is widely used to determine a drug's efficacy (Aykul & Martinez-Hackert 2016). The IC_{50} for MB, GO-MB, and rGO-MB were determined and compared with the chemotherapy drug, 5-FU, as the positive control (Figure 4). The IC_{50} curves showed a 50% reduction in cellular viability for the positive inhibitor 5-FU, GO-MB, rGO-MB, and MB. The values were presented as mean ± SD (n = 6).

By comparing the IC_{50} values of the positive control, 5-FU, with those of GO-MB, rGO-MB- MB and MB, it was evident that all the tested compounds were less potent than 5-FU in reducing the viability of MCF-7 cells (Table 2). Among the tested compounds, GO-MB

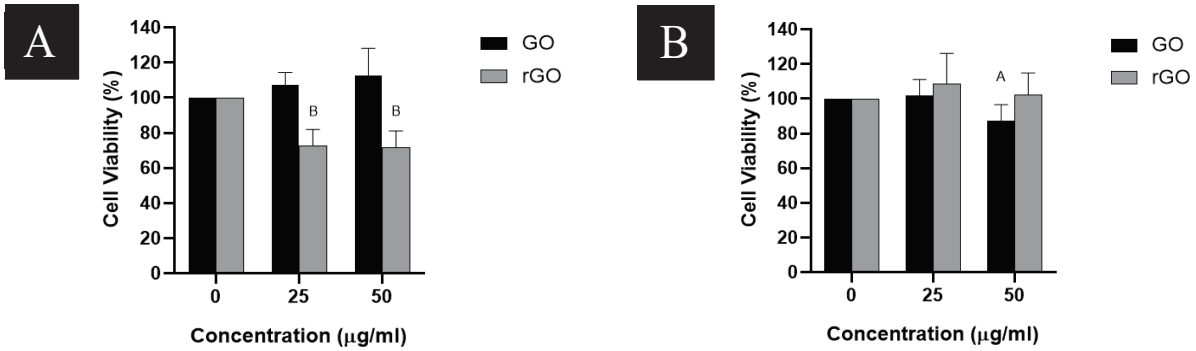

FIGURE 3. The cytotoxicity of GO and rGO on Hs27 (A) and MCF-7 cells (B). Data are presented as mean ± SD (n = 6). The significant difference was analyzed *via* Student's *t*-test (A: $p < 0.01$, B: $p < 0.001$ vs. control) on the cell viability reduction

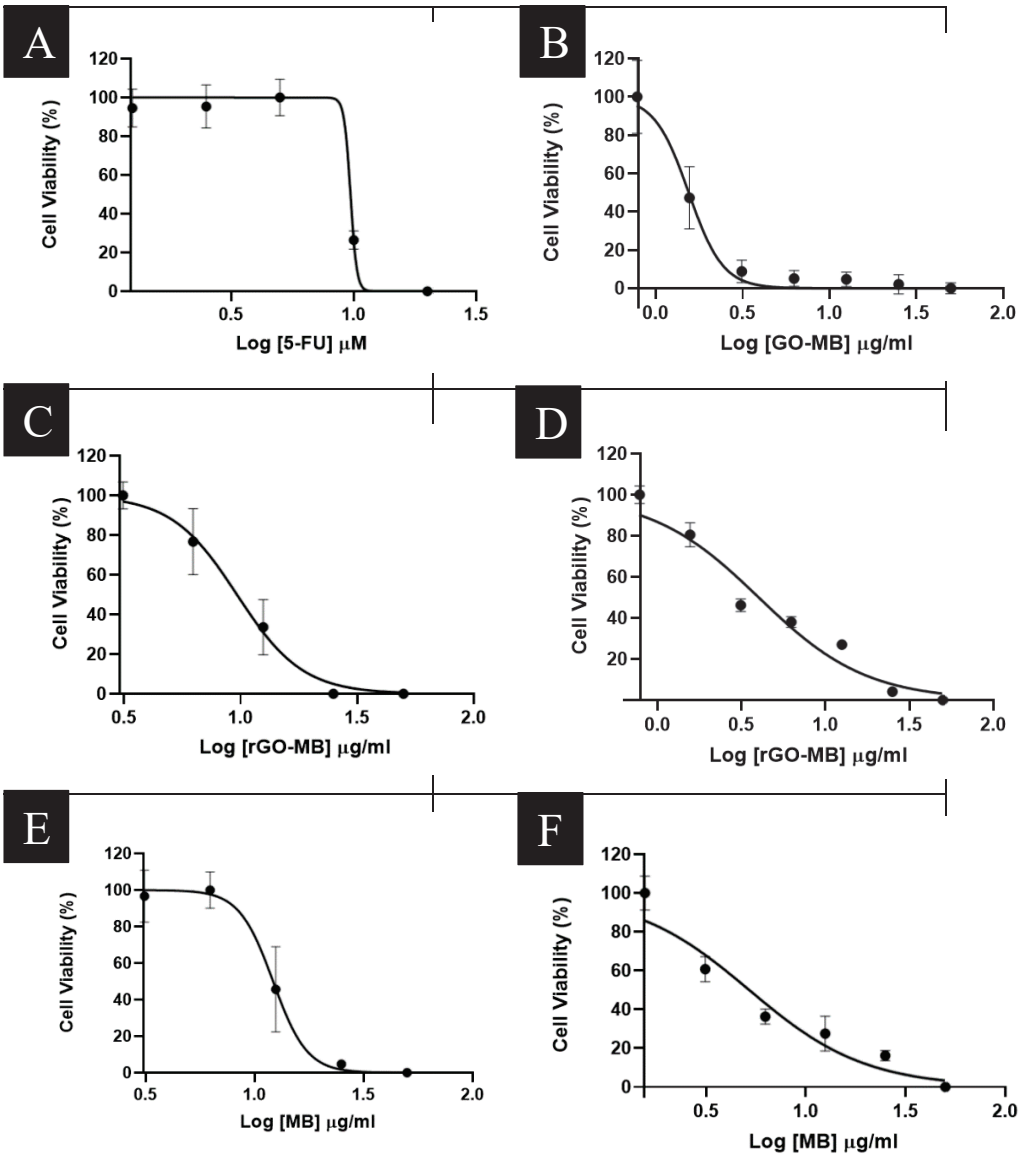

FIGURE 4. The IC_{50} curves of (A) 5-FU (positive control) on MCF-7 cells; (B) GO-MB on MCF-7 cells; (C) rGO-MB on Hs27 cells; (D) rGO-MB on MCF-7 cells; (E) MB on Hs27 cells; and (F) MB on MCF-7 cells. Results were presented as mean ± SD (n = 6)

showed the highest potency, with an IC_{50} of 1.54 μg/mL. Cytotoxicity assessment on Hs27 fibroblast cells showed that all compounds exhibited low toxicity, with GO-MB showing the lowest cytotoxic effect. The IC_{50} value for GO-MB on Hs27 cells was recorded at above 50 μg/mL, indicating a negligible impact on cell viability. Therefore, GO-MB can be considered biocompatible with Hs27 cells. Overall, the results showed that GO-MB has a high potency against MCF-7. A high potency against Hs27 cells could be correlated with potential toxicity in healthy cells. Hence, GO-MB may be more favorable as compared to rGO-MB due to its better effectiveness in killing cancer cells with improved biocompatibility in normal cells.

Figure 5 illustrates the toxicity of GO-MB, rGO-MB, and MB on Hs27 and MCF-7 cells at different concentrations. The comparison between the control group and GO-MB at lower concentrations of 3.125 and 6.25 μg/mL showed insignificant cytotoxicity on Hs27 cells, while at higher concentrations, GO-MB exhibited more toxicity (12.5 to 50 μg/mL, $p < 0.001$). However, both rGO-MB and MB showed significant differences across the concentrations tested when compared with the control group in Hs27 cells ($p < 0.001$). Between GO-MB and MB, significant differences were observed from 3.125 to 50 μg/mL (3.125 μg/mL: $p < 0.05$, 6.25 μg/mL: $p < 0.01$, 12.5 to 50 μg/mL: $p < 0.001$), while for the comparison between rGO-MB and MB, no significant difference could be observed at 3.125 μg/mL, while at the concentrations of 6.25 μg/mL ($p < 0.001$) and 12.5 μg/mL ($p < 0.05$) showed significant differences. Hs27 cells were completely suppressed following treatment with rGO-MB at 25 and 50 μg/mL (Figure 5(A)).

On the other hand, all groups (GO-MB, rGO-MB, and MB) showed significant differences ($p < 0.001$) in MCF-7 when compared with the control (Figure 5(B)). At a low concentration of 3.125 μg/mL, both GO-MB and rGO-MB exhibited a significant difference when compared to MB ($p < 0.001$) and the MCF-7 cell viability was reduced to 25% and 28%, respectively. rGO-MB showed higher toxicity in the concentration range between 12.5 μg/mL and 50 μg/mL when compared to GO-MB and MB. Among the three test compounds, GO-MB was able to reduce the highest percentage of MCF-7 cell viability when tested with the lowest concentration of 3.125 μg/mL, followed by rGO-MB, indicating the effectiveness of GO-MB and rGO-MB in killing breast cancer cells.

GO-MB was significantly cytotoxic towards MCF-7 cells across the concentrations tested compared to Hs27 ($p < 0.001$), even at a low concentration of 3.125 μg/mL (Figure 6(A)). On the other hand, rGO-MB exhibited significant cytotoxicity towards MCF-7 cells when compared to Hs27 at both concentrations of 3.125 and 6.25 μg/mL ($p < 0.001$), while no significant difference could be observed at higher concentrations (Figure 6(B)).

Between GO-MB, rGO-MB, and MB, GO-MB was able to control the release of MB efficiently to target breast cancer cells without giving significant cytotoxicity towards Hs27 cells. The results suggested that GO may be preferable for the drug delivery of hydrophilic MB to target breast cancer cells as compared to rGO, as it showed enhanced biocompatibility in non-cancerous cell lines as well as improved effectiveness in the killing of breast cancer cells, even at a low concentration of 3.125 μg/mL.

According to previous studies, GO has been shown to inhibit the formation of tumor spheres in various cancer cell lines, including ovarian, breast, and lung cancers. This effect is believed to be mediated through the activation of toll-like receptor (TLR) signaling pathways, which subsequently induce autophagy and exert antitumor activity (Priyadarsini et al. 2018). In addition, human solid tumors are known to exhibit a glycolytic phenotype that results in an acidic extracellular microenvironment. This acidity is driven by hypoxia and leads to a pH gradient that promotes the uptake of weak acids and limits the accumulation of weak bases in tumor tissues (Adams & Morgan 2011). As GO contains carboxylic acid groups that contribute to its acidic nature, it is plausible that GO may be preferentially internalized by cancer cells. This hypothesis is consistent with the cytotoxicity results obtained in this study, in which GO exhibited a pronounced cytotoxic effect against MCF-7 breast cancer cells.

Furthermore, the biocompatibility of GO is enhanced by the presence of oxygen-containing functional groups introduced during the oxidation process, which increase its hydrophilicity and improve its suitability for biomedical applications as compared to rGO that is more hydrophobic (Alam et al. 2020). In contrast, rGO exhibited greater cytotoxicity, likely due to the restoration of the pristine graphene-like structure during reduction. This process eliminates oxygen functionalities and repair lattice defects, resulting in a more graphite-like surface. Exposure of cells to the hydrophobic rGO may have triggered the generation

TABLE 2. The IC_{50} values of 5-FU (positive control), GO-MB, rGO-MB, and MB were tested on Hs27 and MCF-7 cells

Test compounds	IC_{50} (μg/mL) MCF-7 cells	IC_{50} (μg/mL) Hs27 cells
5-FU	1.26	> 2.6 (> 20 μM)
MB	5.19	12.15
GO-MB	1.54	> 50
rGO-MB	3.99	9.64

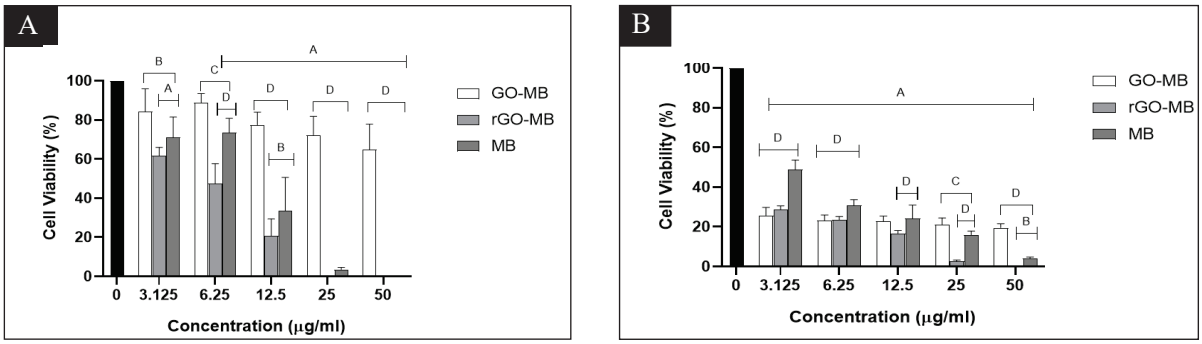

FIGURE 5. The cytotoxicity of GO-MB, rGO-MB and MB on Hs27 (A) and MCF-7 cells (B) tested at different concentrations (3.125, 6.25, 12.5, 25 and 50 μg/mL). The results are presented as mean ± SD (n = 6). The significance of the results was determined using two-way ANOVA followed by the Bonferroni post-hoc test. A to D represented the significant difference between each group (A: $p < 0.001$ vs. control; B: $p < 0.05$, C: $p < 0.01$, D: $p < 0.001$ vs. MB) on the cell viability reduction

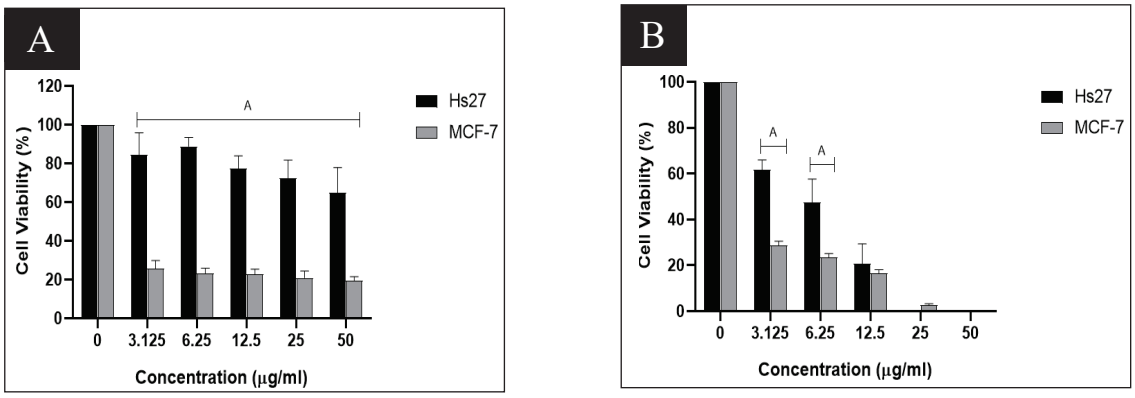

FIGURE 6. The comparison between cytotoxicity of GO-MB (A) and rGO-MB (B) at different concentrations (3.125, 6.25, 12.5, 25 and 50 μg/mL) on Hs27 and MCF-7 cells. Data are presented as mean ± SD (n = 6). Significant difference was analyzed *via* two-way ANOVA and Bonferroni post-hoc test. A represented the significant difference between each group (A: $p < 0.001$ vs. Hs27) in the cell viability reduction

of intracellular reactive oxygen species in a dose- and time-dependent manner, thereby explaining the higher cytotoxic effect observed in Hs27 cells in this study (De Silva, Huang & Yoshimura 2018; Gurunathan et al. 2013).

A previous study proposed that pristine graphene may cause cytotoxic effect by disrupting mitochondrial membrane potential and triggering apoptosis via the mitochondrial pathway (Li et al. 2012). Moreover, several studies have linked the cytotoxicity of graphene-based materials to oxidative stress and the physical interaction between the sharp edges of graphene and the cellular membrane which can lead to membrane damage and cell death (Akhavan & Ghaderi 2010; Chang et al. 2011; Gurunathan et al. 2013). Despite these findings, Alam et al. (2020) reported that both GO and rGO exhibited minimal cytotoxicity, with GO showing even higher levels of cell viability, highlighting the importance of material preparation and contextual conditions in determining cytotoxic outcomes.

MB has demonstrated cytotoxicity towards both Hs27 and MCF-7. Previous studies have reported that MB exhibits cytotoxic effects at concentrations exceeding 20 μM due to its ability to traverse cellular membranes – facilitated by its aromatic ring structure – and accumulate within mitochondria, lysosomes, and double-stranded DNA (Salahuddin et al. 2021). MB's increased cytotoxicity at higher concentrations, particularly in MCF-7 cells, aligns with the findings of this study. The cytotoxic mechanism may involve inhibition of soluble guanylate cyclase and NAD+ oxidation (Khanal, Ngoc Bui & Seo 2014), as well as potential intercalation with purine nucleotides that leads to DNA helical unwinding. Notably, the incorporation of MB into GO was shown to mitigate its inherent cytotoxicity, enhancing overall cellular compatibility. This suggests that GO-MB complexes could represent a promising approach in the development of targeted therapeutics for breast cancer treatment (Salahuddin et al. 2021).

CONCLUSION

GO and rGO were successfully synthesized from graphite, and the loading of MB onto the GO and rGO was confirmed by FT-IR analysis. The *in vitro* release study showed the ability of GO to control the release of MB under acidic conditions. The release of MB from rGO was faster as compared to GO, suggesting the interaction of MB with rGO was probably through weak hydrophobic interaction. The cytotoxic study for GO, GO-MB, rGO, rGO-MB, and MB was investigated in human fibroblast cell lines (Hs27) and breast cancer cell lines (MCF-7). GO-MB was considered a much safer option as compared to rGO-MB and MB by referring to the SI, which supported the potential of GO to eliminate tumor cells with a lower cytotoxic effect on healthy cells. Overall, GO as a drug carrier may be a preferable option to deliver MB for anti-breast cancer treatment due to its advantages, including the ability to load a higher amount of MB than rGO, the controlled release of MB under acidic conditions, and the selective killing of cancerous cells with less cytotoxicity on normal cells.

ACKNOWLEDGEMENTS

This study was supported financially by the Ministry of Higher Education (MOHE), Malaysia under the Fundamental Research Grant Scheme (FRGS) (Grant Number FRGS/1/2022/STG01/USM/02/5).

REFERENCES

Adams, D.J. & Morgan, L.R. 2011. Tumor physiology and charge dynamics of anticancer drugs: Implications for camptothecin-based drug development. *Current Medicinal Chemistry* 18(9): 1367-1372.

Akhavan, O. & Ghaderi, E. 2010. Toxicity of graphene and graphene oxide nanowalls against bacteria. *ACS Nano* 4(10): 5731-5736.

Alam, K., Jo, Y.Y., Park, C.K. & Cho, H. 2020. Synthesis of graphene oxide using atmospheric plasma for prospective biological applications. *International Journal of Nanomedicine* 15: 5813-5824.

Andrijanto, E., Shoelarta, S., Subiyanto, G. & Rifki, S. 2016. Facile synthesis of graphene from graphite using ascorbic acid as reducing agent. *AIP Conference Proceedings.* 2016: 020003.

Arias, F.A., Guevara, M., Tene, T., Angamarca, P., Molina, R., Valarezo, A., Salguero, O., Gomez, C.V., Arias, M. & Caputi, L.S. 2020. The adsorption of methylene blue on eco-friendly reduced graphene oxide. *Nanomaterials* 10(4): 681.

Asif Mohd Itoo, Sree Lakshmi Vemula, Mahima Tejasvni Gupta, Mahesh Vilasrao Giram, Sangishetty Akhil Kumar, Balaram Ghosh & Swati Biswas. 2022. Multifunctional graphene oxide nanoparticles for drug delivery in cancer. *Journal of Controlled Release* 350: 26-59.

Azizighannad, S. & Mitra, S. 2018. Stepwise reduction of graphene oxide (GO) and its effects on chemical and colloidal properties. *Scientific Reports* 8(1): 10083.

Botas, C., Álvarez, P., Blanco, P., Granda, M., Blanco, C., Santamaría, R., Romasanta, L.J., Verdejo, R., López-Manchado, M.A. & Menéndez, R. 2013. Graphene materials with different structures prepared from the same graphite by the Hummers and Brodie methods. *Carbon* 65: 156-164.

Chang, Y., Yang, S.T., Liu, J.H., Dong, E., Wang, Y., Cao, A., Liu, Y. & Wang, H. 2011. *In vitro* toxicity evaluation of graphene oxide on A549 cells. *Toxicology Letters* 200(3): 201-210.

Chasanah, U., Trisunaryanti, W., Oktaviano, H.S., Triyono, T. & Fatmawati, D.A. 2022. Role of temperature and exposure time for controlled and accelerated synthesis of graphene oxide using tour method. *Indonesian Journal of Chemistry* 22(5): 1205-1217.

De Silva, K.K.H., Huang, H.H. & Yoshimura, M. 2018. Progress of reduction of graphene oxide by ascorbic acid. *Applied Surface Science* 447: 338-346.

Faniyi, I.O., Fasakin, O., Olofinjana, B., Adekunle, A.S., Oluwasusi, T.V., Eleruja, M.A. & Ajayi, E.O.B. 2019. The comparative analyses of reduced graphene oxide (RGO) prepared via green, mild and chemical approaches. *SN Applied Sciences* 1(10): 1181.

Farmoudeh, A., Akbari, J., Saeedi, M., Ghasemi, M., Asemi, N. & Nokhodchi, A. 2020. Methylene blue-loaded niosome: Preparation, physicochemical characterization, and *in vivo* wound healing assessment. *Drug Delivery and Translational Research* 10(5): 1428.

Ghasemi, M., Turnbull, T., Sebastian, S. & Kempson, I. 2021. The MTT assay: Utility, limitations, pitfalls, and interpretation in bulk and single-cell analysis. *International Journal of Molecular Sciences* 22(23): 12827.

Goldstein, J.I., Newbury, D.E., Michael, J.R., Ritchie, N.W.M., Scott, J.H.J. & Joy, D.C. 2017. *Scanning Electron Microscopy and X-Ray Microanalysis.* New York: Springer.

Gurunathan, S., Han, J.W., Eppakayala, V. & Kim, J.H. 2013. Green synthesis of graphene and its cytotoxic effects in human breast cancer cells. *International Journal of Nanomedicine* 8: 1015-1027.

Habte, A.T. & Ayele, D.W. 2019. Synthesis and characterization of reduced graphene oxide (rGO) started from graphene oxide (GO) using the tour method with different parameters. *Advances in Materials Science and Engineering* 2019: 5058163.

Hidayah, N.M.S., Liu, W.W., Lai, C.W., Noriman, N.Z., Khe, C.S., Hashim, U. & Lee, H.C. 2017. Comparison on graphite, graphene oxide and reduced graphene oxide: Synthesis and characterization. *AIP Conference Proceedings.* 2017: 150002.

Hoseini-Ghahfarokhi, M., Mirkiani, S., Mozaffari, N., Abdolahi Sadatlu, M.A., Ghasemi, A., Abbaspour, S., Akbarian, M., Farjadian, F. & Karimi, M. 2020. Applications of graphene and graphene oxide in smart drug/gene delivery: Is the world still flat? *International Journal of Nanomedicine* 15: 9469-9496.

Joyce Nirmala, M., Kizhuveetil, U., Johnson, A., Balagi, G., Nagarajan, R. & Muthuvijayan, V. 2023. Cancer nanomedicine: A review of nano-therapeutics and challenges ahead. *RSC Adv.* 13: 8606-8629.

Kasturi Muthoosamy, Ibrahim Babangida Abubakar, Renu Geetha Bai, Hwei-San Loh & Sivakumar Manickam. 2016. Exceedingly higher co-loading of curcumin and paclitaxel onto polymer-functionalized reduced graphene oxide for highly potent synergistic anticancer treatment. *Scientific Report* 6: 32808.

Kaur, A., Babaliari, E., Bolanos-Garcia, V.M., Kefalogianni, M., Psilodimitrakopoulos, S., Kavatzikidou, P., Ranella, A., Ghorbani, M., Stratakis, E., Eskin, D.G. & Tzanakis, I. 2025. Assessment of aqueous graphene as a cancer therapeutics delivery system. *Scientific Report* 15: 15396.

Khanal, A., Ngoc Bui, M.P. & Seo, S.S. 2014. Microgel-encapsulated methylene blue for the treatment of breast cancer cells by photodynamic therapy. *Journal of Breast Cancer* 17(1): 18-24.

Kim, E., Qin, X., Qiao, J.B., Zeng, Q., Fortner, J.D. & Zhang, F. 2020. Graphene oxide/mussel foot protein composites for high-strength and ultra-tough thin films. *Scientific Reports* 10: 19082.

Li, Y., Liu, Y., Fu, Y., Wei, T., Le Guyader, L., Gao, G., Liu, R.S., Chang, Y.Z. & Chen, C. 2012. The triggering of apoptosis in macrophages by pristine graphene through the MAPK and TGF-beta signaling pathways. *Biomaterials* 33(2): 402-411.

Liu, L., Ma, Q., Cao, J., Gao, Y., Han, S., Liang, Y., Zhang, T., Song, Y. & Sun, Y. 2021. Recent progress of graphene oxide-based multifunctional nanomaterials for cancer treatment. *Cancer Nanotechnology* 12: 18.

Ma, M., Cheng, L., Zhao, A., Zhang, H. & Zhang, A. 2020. Pluronic-based graphene oxide-methylene blue nanocomposite for photodynamic/photothermal combined therapy of cancer cells. *Photodiagnosis and Photodynamic Therapy* 29: 101640.

Marcano, D.C., Kosynkin, D.V., Berlin, J.M., Sinitskii, A., Sun, Z., Slesarev, A., Alemany, L.B., Lu, W. & Tour, J.M. 2010. Improved synthesis of graphene oxide. *ACS Nano* 4(8): 4806-4814.

Martis, L.J., Parushuram, N. & Sangappa, Y. 2022. Preparation, characterization, and methylene blue dye adsorption study of silk fibroin–graphene oxide nanocomposites. *Environmental Science: Advances* 1(3): 285-296.

National Cancer Institute. 2025. Side Effects of Cancer Treatment - NCI. Retrieved June 16, 2026. https://www.cancer.gov/about-cancer/treatment/side-effects

Priyadarsini, S., Mohanty, S., Mukherjee, S., Basu, S. & Mishra, M. 2018. Graphene and graphene oxide as nanomaterials for medicine and biology application. *Journal of Nanostructure in Chemistry* 8(2): 123-137.

Ramachandran, P., Khor, B.K., Lee, C.Y., Doong, R.A., Oon, C.E., Thanh, N.T.K. & Lee, H.L. 2022. N-doped graphene quantum dots/titanium dioxide nanocomposites: A study of ROS-forming mechanisms, cytotoxicity and photodynamic therapy. *Biomedicines* 10(2): 421.

Sakin Omer, O., Hussein, M.A., Hussein, B.H.M. & Mgaidi, A. 2018. Adsorption thermodynamics of cationic dyes (methylene blue and crystal violet) to a natural clay mineral from aqueous solution between 293.15 and 323.15 K. *Arabian Journal of Chemistry* 11(5): 615-623.

Salahuddin, N., Akelah, A., Elnagar, M. & Abdelwahab, M.A. 2021. Antibacterial and cytotoxicity of methylene blue loaded-cellulose nanocarrier on breast cancer cell line. *Carbohydrate Polymer Technologies and Applications* 2: 100138.

Senem Aykul & Erik Martinez-Hackert. 2016. Determination of half-maximal inhibitory concentration using biosensor-based protein interaction analysis. *Analytical Biochemistry*. 508: 97-103. https://doi.org/10.1016/j.ab.2016.06.025.

Tewatia Krishna, Anuradha Sharma, Mamta Sharma & Arun Kumar. 2021. Synthesis of graphene oxide and its reduction by green reducing agent. *Materials Today* 44(6): 3933-3938.

van Oss, C.J. 2008. The properties of water and their role in colloidal and biological systems. *Interface Science and Technology*. New York: State University of New York at Buffalo 1-224.

World Health Organization (WHO). 2024. *Breast Cancer.* March 13. https://www.who.int/news-room/fact-sheets/detail/breast-cancer?utm_source=chatgpt.com

Wu, L. & Jiang, X. 2018. Proton transfer at the interaction interface of graphene oxide. *Analytical Chemistry* 90(17): 10223-10230.

Yaghoubi, F., Motlagh, N.S.H., Naghib, S.M., Haghiralsadat, F., Jaliani, H.Z. & Moradi, A. 2022. A functionalized graphene oxide with improved cytocompatibility for stimuli-responsive co-delivery of curcumin and doxorubicin in cancer treatment. *Scientific Report* 12: 1959.

Yanikoglu, R., Karakas, C.Y., Ciftci, F., Insel, M.A., Karavelioglu, Z., Varol, R., Yilmaz, A., Cakir, R., Uvet, H. & Ustundag, C.B. 2024. Development of graphene oxide-based anticancer drug combination functionalized with folic acid as nanocarrier for targeted delivery of methotrexate. *Pharmaceutics* 16(6): 837.

Zaaba, N.I., Foo, K.L., Hashim, U., Tan, S.J., Liu, W.W. & Voon, C.H. 2017. Synthesis of graphene oxide using modified hummers method: Solvent influence. *Procedia Engineering* 184: 469-477.

Zhang, L., Xia, J., Zhao, Q., Liu, L. & Zhang, Z. 2010. Functional graphene oxide as a nanocarrier for controlled loading and targeted delivery of mixed anticancer drugs. *Small* 6(4): 537-544.

Zhao, P., Fan, X., Zhang, Q., Wang, X., Zhang, M., Ran, J., Lv, D., Liu, J., Shuai, J. & Wu, H. 2019. The effect of hydration on pores of shale oil reservoirs in the third submember of the Triassic Chang 7 member in southern Ordos basin. *Energies* 12(20): 3932.

*Corresponding author; email: amirahmg@usm.my